HHS Public Access

Author manuscript

Int J Cancer. Author manuscript; available in PMC 2021 October 15.

Published in final edited form as:

Int J Cancer. 2020 October 15; 147(8): 2279–2292. doi:10.1002/ijc.33050.

Blockade of p38 kinase impedes the mobilization of pro-tumorigenic myeloid populations to impact breast cancer metastasis

Justin Zonneville[1], **Sean Colligan**[2], **Sydney Grant**[1], **Alexandra Miller**[5], **Paul Wallace**[3], **Scott I. Abrams**[2,*], **Andrei V. Bakin**[1,4,*]

[1]Department of Cancer Genetics and Genomics, Roswell Park Comprehensive Cancer Center, Buffalo, New York 14263

[2]Department of Immunology, Roswell Park Comprehensive Cancer Center, Buffalo, New York 14263

[3]Department of Flow & Image Cytometry, Roswell Park Comprehensive Cancer Center, Buffalo, New York 14263

[4]Sechenov Medical University, Moscow, Russia 119991

[5]Drake University, Des Moines, Iowa 50311

Abstract

Patients with metastatic breast cancer (MBC) have limited therapeutic options and novel treatments are critically needed. Prior research implicates tumor-induced mobilization of myeloid cell populations in metastatic progression, as well as being an unfavorable outcome in MBC; however, the underlying mechanisms for these relationships remain unknown. Here, we provide evidence for a novel mechanism by which p38 promotes metastasis. Using triple-negative breast cancer models, we showed that a selective inhibitor of p38 (p38i) significantly reduced tumor growth, angiogenesis, and lung metastasis. Importantly, p38i decreased the accumulation of

[*]**CORRESPONDING AUTHORS:** Andrei V. Bakin, Department of Cancer Genetics and Genomics, Tel. (716) 845-1033; andrei.bakin@roswellpark.org; and Scott I. Abrams, Department of Immunology, Tel. (716) 845-4375, scott.abrams@roswellpark.org Roswell Park Comprehensive Cancer Center, Buffalo, New York 14263.

AUTHOR CONTRIBUTIONS

A.V.B. and S.I.A. conceived and designed the experiments, J.Z., S.C., S.G., and A.M. performed the experiments and analyzed the data; A.V.B. and S.I.A. analyzed and interpreted the data, P.W. helped in the analysis and interpretation of the Luminex data; A.V.B., S.I.A., S.C., and J.Z., contributed to preparing and writing the paper.

DISCLOSURE OF INTEREST

The authors report no conflict of interest

DATA ACCESSIBILITY

The heat-map data that support the findings of this study are generated using the cBIoportal for Cancer Genomics at http://www.cbioportal.org/ and the breast cancer TCGA dataset (Project ID: TCGA-BRCA; dbGaP Study Accession: phs000178) available in a public repository the Genomic Data Commons Data Portal at https://portal.gdc.cancer.gov/. The mouse expression data were derived from the GEO dataset GSE62817, and human expression data of breast cancer stromal compartments were derived from the dataset GSE12622; both datasets are available in the public domain of the NCBI Gene Expression Omnibus at https://www.ncbi.nlm.nih.gov/geo/. All the other data supporting the findings of this study are available within the article and its Supplementary Information files and from the corresponding author upon reasonable request.

ETHIC STATEMENT

A study protocol and guidelines approved by the Institute Animal Care and Use Committee (IACUC). The facility is certified by the American Association for Accreditation of Laboratory Animal Care (AAALAC) and in accordance with current regulation and standards of the US Department of Agriculture and the US Department of Health and Human Services.

myeloid populations, namely myeloid-derived suppressor cells (MDSCs) and CD163$^+$ tumor-associated macrophages (TAMs). p38 controlled the expression of tumor-derived chemokines/cytokines that facilitated the recruitment of pro-tumor myeloid populations. Depletion of MDSCs was accompanied by reduced TAM infiltration and phenocopied the anti-metastatic effects of p38i. Reciprocally, p38i increased tumor infiltration by cytotoxic CD8$^+$ T cells. Furthermore, the CD163$^+$/CD8$^+$ expression ratio inversely correlated with metastasis-free survival in breast cancer, suggesting that targeting p38 may improve clinical outcomes. Overall, this study highlights a previously unknown p38-driven pathway as a therapeutic target in MBC.

Keywords

breast cancer; metastasis; myeloid-derived suppressor cells; macrophages; p38 kinase; tumor microenvironment

INTRODUCTION

Breast cancer (BC) is the second-leading cause of cancer-related death in women [1]. Among BC subtypes, triple-negative breast cancer (TNBC, ER/PR/HER2-negative) poses significant challenges due to early onset and a lack of targeted therapies. The current standard-of-care for TNBC is chemotherapy with anthracyclines and taxanes, achieving pathological complete response rates (pCRs) of nearly 40% [2]. Despite high response rates, a significant number of TNBC patients develop metastatic disease with worse overall survival than those with other subtypes [3], suggesting a pressing need for newer therapeutic options. Evidence points to the tumor microenvironment (TME) as a major contributing factor to unfavorable outcomes. Remarkably, TNBC is enriched with stromal components [4], including mesenchymal stromal cells (MSCs) and immune populations, many of which paradoxically support cancer progression [5]. Current efforts in the field are directed towards identifying druggable targets in the TME.

Tumor and stromal cells in the TME are engaged in complex and dynamic interactions that drive tumor angiogenesis and immune-resistant phenotypes [5]. Prior studies, including ours, indicate that cancer cells alter the behavior of MSCs, especially cancer-associated fibroblasts (CAFs), to promote tumor vasculature and an immune suppressive milieu [5–8]. In particular, the tumor-stroma crosstalk can stimulate the expansion of tumor-associated macrophages (TAMs) and myeloid-derived suppressor cells (MDSCs) [9]. These myeloid populations have been recently linked to the formation of the pre-metastatic niche [10, 11], a tumor-induced permissive microenvironment at distal sites [12]. Thus, the molecular pathways controlling tumor-induced recruitment or expansion of myeloid cell populations, such as TAMs and MDSCs, may serve as potential therapeutic targets [13–15].

Significant activation of the p38 mitogen-activated protein kinase (p38 MAPK; henceforth referred to p38) was reported for the breast and lung TMEs [6, 7, 16]. Earlier work showed that p38 contributes to the invasive and metastatic phenotype of TNBC [17, 18]. Furthermore, genetic inactivation of p38 in cancer cells reduced tumor angiogenesis [6, 19]. Recently, TAK1-p38 signaling was linked to metastasis of TNBC to the lung in preclinical models, while the mechanism remained unknown [20]. Notably, clinical data indicate significant

activation of p38 in breast tumors and its association with disease progression [21], further implicating p38 as a potential therapeutic target in the breast TME. Among the four p38 MAPK family members, the p38-α kinase encoded by the *MAPK14* gene is ubiquitously expressed at high levels [22]. Investigational agents inhibiting p38-α/β isoforms showed promising results in pre-clinical models [18, 23] and were tested clinically for the treatment of chronic inflammation [24]. However, little is known about their impact on the breast TME and their ability to inhibit metastasis of breast cancer to the lungs, a major site of tumor dissemination.

In this study, we tested the hypothesis that p38 drives TNBC growth and metastasis through orchestration of a pro-tumorigenic myeloid-dependent mechanism. Our data revealed that single-agent treatment with a selective p38 inhibitor (p38i) significantly reduced tumor growth and lung metastases. Mechanistic studies showed that p38i reduced tumor angiogenesis, as well as mobilization of pro-tumor myeloid cells to the TME and distal organs. Importantly, we found that p38 controlled tumor-induced recruitment and expansion of pro-tumor TAMs and MDSCs. Depletion of MDSCs, which was accompanied by a reduction in TAMs, mimicked the response to p38i. These findings indicate that p38 is a viable therapeutic target in the breast TME and suggest that agents that block p38 inhibit lung metastasis by impeding the recruitment of pro-tumor myeloid populations.

METHODS

Cell lines and culture conditions

Mouse mammary carcinoma 4T1 (RRID:CVCL_0125), metastatic breast cancer MDA-MB-231 (RRID:CVCL_0062), and human embryonic fibroblast WI-38 (RRID:CVCL_0579) cell lines were obtained from American Type Culture Collection (ATCC, Manassass, VA, USA), and cultured as recommended by ATCC. AT-3 cell line (RRID:CVCL_VR89) was generated by Dr. Scott Abrams (RPCI) from a mammary carcinoma of MMTV-PyMT transgenic C57BL/6 mice [13]. 4T1 and AT-3 cell lines were further engineered to express a Luciferase reporter (4T1-Luc; AT-3-Luc) for detailed bioluminescence tracking of tumor progression. MDA-MB-231-CTR and MDA-MB-231-dnp38 cells expressing EGFP (CTR) or EGFP and Flag-tagged kinase-inactive p38-AGF (dnp38) were generated by retroviral transduction followed by cell sorting, and are described elsewhere [17]. All human cell lines were authenticated using short tandem repeat profiling by ATCC or the Roswell Park Core within the last three years. The cells were routinely screened for mycoplasma, and all studies made use of mycoplasma-free cells. Cell cultures were supplemented with 10% heat-inactivated fetal bovine serum (FBS) and penicillin/streptomycin at 37°C with 5–10% CO_2 in a humidified incubator.

p38 inhibitor, Antibodies and Other Reagents

The information is presented in Supplementary Information.

Mice

Female BALB/c or C57BL/6 mice (6–7 week old) were from the Charles River Laboratories (Wilmington, MA). Female SCID/CB17 mice were from a colony of SCID/CB17 mice bred

and maintained at the Animal Facility of the Roswell Park (RP). Animals were kept in microinsulator units and provided with food and water *ad libitum* according to a protocol and guidelines approved by the Institute Animal Care and Use Committee (IACUC). The facility is certified by the American Association for Accreditation of Laboratory Animal Care (AAALAC) and in accordance with current regulation and standards of the US Department of Agriculture and the US Department of Health and Human Services.

Mice were inoculated into the mammary fat pad with exponentially growing 4T1-Luc or AT-3-Luc tumor cells in Dulbecco's Phosphate Buffered Saline (DPBS) (50–200,000/mouse). Control naïve mice were injected with DPBS only. At day 4 post inoculation, mice were randomly divided into three groups with 8 mice/group: Naïve, tumor-bearing (TB), and TB+p38i. Inhibitor of p38, Ralimetinib [25], was given at 30mg/kg by oral gavage for 9 consecutive days, while Naïve and TB groups (4T1-luc or AT-3-Luc) received DPBS. In the study with 50,000 4T1-Luc cells (Fig. 1), Ralimetinib was administered by oral gavage starting on day 14 post implantation, when the tumor size reached ~100mm^3; at study endpoint on day 34 mice were subjected to Bioluminescence Imaging. Mouse weight was measured two times per week. Tumor diameters were measured with electronic calipers twice/week. Volumes were calculated using the formula (length) × (width)^2/2. On days 7 and 14, mice were subjected to Bioluminescence Imaging (see below). At endpoint on day 14, mice were euthanized and subjected to necropsy and organ collection. Blood was collected for CBC by cardiac puncture.

For MDSC depletion studies, 4T1-Luc cells were othotopically inoculated into BALB/c mice (six per group), followed by i.p. injections with anti-Ly6G (clone 1A8) or an appropriate isotype-control antibody (rat IgG2a) each at 100μg/mouse (Bio X Cell, Lebanon, NH) every other day for two weeks. At day 14, the mice were subjected to bioluminescence imaging and tissue collection as above. For the established tumor model, when tumor reached ~100mm^3, mice were randomly divided into two groups with 8 mice/group, and p38i was given daily by oral gavage at 30mg/kg. At day 14, mice were analyzed as above.

Bioluminescence Assays

Bioluminescence imaging was done on days 7 and 14. D-luciferin (100 μL, 15 mg/ml) was injected intraperitoneally ~10 min prior to imaging. Luminescence was measured in IVIS Spectrum (S10OD16450) and analyzed using Living Image software, reported as average flux (photons/second). Bioluminescence assays were done on protein extracts from the lungs and livers using the VERITAS microplate luminometer and Luciferase Assay System (Promega, Madison WI). Relative luminescence units (RLU) were determined using the Veritas GLOMAX software, version 1.9.3., and quantified with MS-Excel.

Complete Blood Counts

Blood was collected into EDTA solution to prevent coagulation and then diluted 1:10 with DPBS. Analysis was performed using the HemaTrue Analyzer and HeskaView Integrated Software version 2.5.2.

Immunohistochemistry (IHC)

Tumors, organs or tissues were fixed in 10% (v/v) formalin before embedding in paraffin and staining by the Pathology Core. Blood vessels were stained with anti-mouse CD31 antibody as described [19]. All comparisons were performed on mice with comparably sized tumors. Microvessel density was determined as described [26] and the data were presented as mean number of microvessels/field (0.2 mm^2) ± standard deviation. The Ki-67 staining and analysis were conducted using standard procedures [19]. CD163 staining was processed using ImageScope software version 12.2.1.5005. $CD163^+$ stains were quantified using ImageJ software version 1.52a from three visual fields in three different tumors per group at ×200 magnification. Megakaryocytes in the spleen and myeloid cell foci in the liver were quantified using ImageJ from three fields per sample for each group at ×100. $Ly6G^+$ stains were quantified at ×400 using ImageJ software from three fields in three tumors per group. Tumor tissues from MDA-MB-231 cell xenografts in SCID mice were generated and processed as described [19]; tumor tissues were stained for $F4/80^+$ (total macrophages) and $CD163^+$ macrophages, and processed as above. The mean numbers are shown for each test. Statistical analysis was performed using a two-tailed test with Microsoft Excel.

Immunoblotting

Tumor cells were seeded in a 6-well plate at 300,000 cells/well and treated with various doses of p38i. Whole-cell lysates were prepared using NP40 lysis buffer and processed essentially as described [19]. Snap-frozen tumor tissues were ground and suspended in NP40 lysis buffer.

Luminex Assay

Tumor cell-conditioned media was analyzed using Luminex 200 system for Human Cytokine/Chemokine Panel. Briefly, MDA-MB-231 cells were seeded at 450,000 cells/well. The following day, cells were washed with PBS and replenished with serum-free media. After incubation for 48 hours, the conditioned media was subjected to multiplex analysis of multiple cytokines. Forty-one analytes were measured using human high sensitivity cytokine/chemokine kits (Millipore) as described [27]. For the standard curves, reconstituted standards were serially diluted 1:3 with assay buffer for 9-point curves. Assays were assembled using 96-well plates. Each plate contained samples (in duplicates), standards, and two internal quality controls. Analyte capture and detection was carried out according to manufacturer's instructions. Data were acquired using a Luminex 200 with xPONENT version 3.1 software. Individual analyte concentrations were calculated from standard curves generated with BeadView Analysis Software using a five-point curve fitting routine.

qPCR Analysis

Cells were treated with p38i or vehicle-control (DMSO) and RNA was extracted using the TRIzol Reagent according to the manufacturer's instructions. cDNA samples were prepared and amplified in triplicate using standard protocols with a reference marker 5S rRNA as described in [19]. Primer sequences are presented in Supplementary file.

ELISA

ELISA assays for mouse Ccl2/MCP1 were performed with 4T1-Luc tumor tissues from mice treated with p38i or received DPBS, as well as 4T1-Luc cell conditioned media. Briefly, 4T1-Luc cells were cultured at 300,000 cells/well in 6-well plates, then were washed with DPBS and serum-free media was added to each well with 2μM of p38i or vehicle-control (DMSO). Conditioned media was collected at 48 hours and subjected to the ELISA procedure according to the manufacturer's instructions. Optical density was measured at 450nm and 570nm. Assays were performed in triplicates and the mean values are shown of two independent repeats.

Flow cytometry

For the lungs, cells were isolated from whole lung digested with collagenase and hyaluronidase. For spleen, lungs and bone marrow, cells were isolated from the spleen and lungs by mechanical dissociation, while bone marrow cells were recovered by flushing femurs and tibias with saline. RBCs were lysed with ACK lysing buffer. Cells were stained for 20 minutes at room temperature in FACS buffer (1xPBS with 5% FBS) and washed once with FACS buffer. All samples were analyzed on an LSRFortessa Cytometer (BD Biosciences) running FACSDiva version 6.1.3, and data files were analyzed using FlowJo version 10.

MDSC generation assay *in vitro*

3×10^6 mouse unfractionated bone marrow cells from female C57BL/6 mice were cultured for 4 days in non-tissue culture-treated petri dishes in 10 mL complete RPMI containing 40 ng/mL G-CSF plus 40 ng/mL GM-CSF as described [28]. Vehicle control, 1–5 μM p38i was added to the culture at day 0. Following culture, MDSCs were co-cultured at 1:1 ratio with syngeneic splenocytes pre-stained with CellTrace Violet Dye for 72 hours. Proliferation of co-cultured $CD4^+$ and $CD8^+$ T cells was measured through CTV dye dilution using flow cytometry, as described [28]. The percentage of suppression was calculated by (ΔMFI anti-CD3–stimulated T cells minus ΔMFI co-cultured T cells) divided by ΔMFI anti-CD3-stimulated T cells, where the difference in mean fluorescence intensity (ΔMFI) was calculated by subtraction from unstimulated controls.

Metadata analysis

The Kaplan–Meier curves of recurrence-free survival in BC patients were generated using Kaplan-Meier Plotter with Log-rank test [29]. Metastasis-free survival data were obtained using a published dataset of 295 BC patients [30] and a prognostic *PROGgene V2* tool [31]. Expression of CD8A and CD163 in BC stromal compartments and their association with BC recurrence at 5 years were generated with *Oncomine* online tool https://www.oncomine.org/ using the dataset of the Finak Breast Cancer Study [32], that is deposited in the NCBI Gene Expression Omnibus (GEO) dataset GSE12622. Heat-map of expression profiles was generated with the TCGA BC dataset (Project ID: TCGA-BRCA, dbGaP Study Accession: phs000178) using the cBioPortal Cancer Genomics tool https://www.cbioportal.org/. The expression data of myeloid cell markers in the lungs of 4T1 tumor-bearing and tumor-free mice were generated using the GEO dataset GSE62817 [33].

Statistics

Statistical significance of data comparisons were determined using the Student's unpaired *t*-test with a two-tailed distribution. Statistical significance was achieved when $P<0.05$. Survival was evaluated using the Kaplan-Meier estimator with the log rank test, based on time-to-arrive at a tumor volume of $1cm^3$ using GraphPad Prism 7.

RESULTS

Blockade of p38 reduces mammary tumor growth and metastasis to the lungs

Prior work showed that genetic inactivation of p38 in TNBC cells reduces tumor growth and metastasis [18, 19]. Here, we explored the response to systemic blockade of p38 in the well-characterized 4T1 mouse mammary carcinoma model, in which tumor cells are implanted into the mammary fat pad of syngeneic female BALB/c mice [8, 34–36]. We examined a selective p38 alpha/beta kinase inhibitor (p38i), Ralimetinib [25], which was administered by oral gavage. Treatment with p38i significantly decreased tumor growth by 45% (Fig. 1A–B), as determined by tumor weight at day 34 (Fig. 1C). The mice did not show evidence of overt toxicities on the bases of the absence of changes in body weight and behavior. Evaluation of survival based on time-to-arrive at 1 cm^3 tumor volume showed a statistically significant increase in survival in the p38i-treated group (Fig. 1D; $P<0.01$). Tumor histology showed that p38i reduced the Ki-67 index by 42% (Suppl. Fig.1A–B). In contrast, in cell culture, p38i did not inhibit the proliferation of 4T1 cells, as well as MDA-MB-231 cells, a well-characterized human TNBC cell line model (Suppl. Fig. 1C), at concentrations that effectively decreased phosphorylation of p38 targets MAPKAPK2 and HSP27 (Suppl. Fig. 1D). Notably, genetic inactivation of p38 in MDA-MB-231 cells did not affect cell proliferation *in vitro* [19].

Histological analysis of CD31-stained tumor tissues showed a significant reduction of the blood-vessel density (BVD) in the p38i-treated group (Fig. 1E–F). This response was consistent with the anti-angiogenic effect of genetic inactivation of p38 in tumor cells [19]. 4T1 tumors develop spontaneous metastases to the lungs during the early phase of primary tumor growth [36]. Histological evaluation of the lungs revealed metastases in tumor-bearing (TB) mice (Fig. 1G), and this was confirmed by bioluminescence assays of whole-lung extracts (Fig. 1H). Treatment with p38i reduced lung metastases (Fig. 1H). A decrease in phospho-MAPKAPK2 levels in tumor tissues further confirmed the p38i inhibitory activity *in vivo* (Fig. 1I). Thus, systemic blockade of p38 as a single-agent strategy reduced tumor growth, angiogenesis, and lung metastasis, while it did not inhibit tumor cell growth *in vitro*.

Inhibition of p38 impedes tumor angiogenesis at early stages of tumor growth

To gain mechanistic insights, we explored the response to p38i in a model of the early stages of the metastatic process [33]. In this model, orthotopic growth of 4T1 tumors promotes the formation of a pre-metastatic niche within the lungs and liver, and this is linked to mobilization of pro-tumor myeloid cells [33]. 4T1 cells were inoculated into the mammary fat pad of female mice, followed by daily doses of p38i starting on day 4 (Fig. 2A). On day 14, 4T1-Luc cells were detected at the site of inoculation but not in the lungs, indicating the absence of macro-metastatic lesions (Fig 2B). p38i-treated group showed lower

luminescence signals (Fig 2B–C), concordant with a reduction in tumor weight, although this was not significant (Fig 2D). CD31-staining revealed a significant reduction in the BVD in the p38i-treated group ($P<0.001$), while their tumor sizes were not statistically different (Fig. 2E–G). All subsequent comparisons were performed in mice on comparably sized tumors. Lung histology did not show macro-metastatic lesions in all experimental groups. The difference in Ki-67 indices between tumor groups (i.e., control *vs.* p38i) did not reach statistical significance. Thus, these data showed that p38i reduced tumor angiogenesis in a pre-metastatic 4T1 tumor setting, which was consistent with genetic inactivation of p38 [19].

Inhibition of p38 reduces infiltration of MDSCs to the lungs and liver

We found a substantial presence of myeloid cells in the blood vessels of TB-mice compared to the lungs from naïve and p38i-treated mice (Suppl. Fig. 2C). Next, we examined the types of myeloid populations, focusing on the granulocytic or polymorphonuclear (PMN) subset of myeloid-derived suppressor cells (MDSCs) [37]. Although MDSCs consist of two major subsets, PMN and monocytic, the 4T1 model is known to induce a robust PMN-MDSC response that contributes to tumor progression [14, 38, 39]. We and others have previously shown that such 4T1 tumor-induced PMN-MDSCs display potent immune suppressive activity [38, 39]. Immunohistochemical (IHC) analysis showed a massive infiltration of PMN-MDSCs, based on Ly6G expression as a canonical marker, into the lungs of TB-mice that is consistent with prior reports [10, 13, 14, 33]. The lung influx of $Ly6G^+$ cells was markedly reduced in the p38i-treated group (Fig. 3A–B) and, interestingly, this was independent of the tumor size (Suppl. Fig. 2B). To validate this finding, we performed flow cytometry on whole-lung tissues for the prototypical $CD11b^+Ly6C^{lo}Ly6G^+$ PMN-MDSC phenotype from TB-mice with comparable tumor sizes (Fig. 3C). Our data showed a significant increase in the level of PMN-MDSCs in the lungs of TB-mice, whereas p38i significantly reduced this response (Fig. 3C). These data indicate that tumor growth provokes the mobilization of PMN-MDSCs to the lungs and p38 kinase plays an important role in this response.

Next, we inspected the histology of the liver, the third most common site of MBC [3]. Histology did not reveal metastatic lesions in the liver (Suppl. Fig. 3A). In contrast, multiple foci of immune cells were readily found within liver sections of TB-mice, while these cells were absent in tumor-free mice (Suppl. Fig. 3A). This tumor-induced immune response was significantly reduced in the p38i-treated group (Suppl. Fig. 3A–B). Further, anti-Ly6G staining revealed PMN-MDSC-like cells within the immune cell foci in the proximity of blood vessels (Suppl. Fig. 3C, yellow arrows). Notably, the $Ly6G^+$ foci were essentially eliminated in the livers of the p38i-treated group (Suppl. Fig. 3C–D). These data indicated that the mammary gland primary tumor instigated the mobilization of myeloid populations, such as PMN-MDSCs, to the lungs and liver, whereas blockade of p38 mitigated this response.

Inhibition of p38 reduces tumor-induced splenomegaly and myelopoiesis

Thus far, we found that p38i decreased tumor-induced mobilization of PMN-MDSCs to the lungs and liver (Fig. 3 and Suppl. Fig. 3). Next, we questioned whether this response involves the spleen, a known site of extramedullary hematopoiesis (EMH) in patients with advanced-stage solid cancers [40] and in TB-mice [35, 41]. Examination of the spleen in TB-

mice revealed a significant increase in organ weight and size (Fig. 3D–E). The analysis of the spleen histology showed expansion of the red-pulp zones, the site of myelopoiesis [42], in TB-mice compared to the control (Fig. 3D). Notably, we found accumulation of megakaryoblasts (MK) in the red-pulp zones of the TB group (Fig. 3D, F), consistent with tumor-induced EMH. The tumor-induced enlargement of the spleen and the expansion of red-pulp zones and MK cells were significantly diminished in the p38i-treated group (Fig. 3D–F). IHC further showed a massive expansion of $Ly6G^+$ cells in the spleen of TB-mice (Fig. 3G), while flow cytometry confirmed a significant increase in the $CD11b^+Ly6C^{lo}Ly6G^+$ population (Fig. 3H). Consistent with this result, we found a significant increase in granulocytes in the peripheral blood (Fig. 3I). Importantly, p38i markedly reduced the expansion of circulating granulocytes and the $Ly6G^+$ cells in the spleen (Fig. 3G–I and Suppl. Fig. 3E). Together, these data revealed that p38 contributes to the tumor-induced expansion of myeloid populations, namely MK and PMN-MDSCs, in the spleens of TB-mice.

p38 controls tumor infiltration by macrophages

TAMs promote tumor angiogenesis and metastasis [10, 15], and high levels of TAMs across a range of solid cancers have been associated with a poor prognosis [43]. Therefore, we examined TAMs in the studied model. First, assessment of peripheral blood showed an up-surge in monocytes in TB-mice, whereas p38i significantly reduced their frequency (Fig. 4A). IHC analysis revealed high levels of $CD163^+$ macrophages in 4T1 tumors, while treatment with p38i significantly reduced the amount of $CD163^+$ TAMs (Fig. 4B–C). CD163 expression has been tied to M2-type macrophages, which promote tumor growth and progression [44, 45].

Next, we tested whether the macrophage influx depends on p38 signaling in tumor cells. To address this question, we utilized a genetic model in which p38 signaling in the TNBC cell line MDA-MB-231 was blocked by a kinase-inactive form of p38-alpha (p38-AGF; dnp38) [19]. IHC of primary tumors showed high levels of $CD163^+$ and total $F4/80^+$ macrophages in empty-vector control tumors, whereas dnp38-tumors showed a significant reduction in TAMs (Fig. 4D). These data showed that genetic inactivation of tumor p38 signaling decreased the mobilization of TAMs to the tumor, while systemic p38i treatment reduced a tumor-driven increase in circulating monocytes and TAMs within the TME.

TAMs and PMN-MDSCs obstruct tumor infiltration by $CD8^+$ cytotoxic T cells [5, 37, 46]. To assess if this mechanism was hampered by p38i, we analyzed tumor infiltration by $CD8^+$ T cells. Staining tumor sections for CD8A, the alpha-chain of the CD8 molecule expressed by cytotoxic T cells, showed a significant increase in $CD8^+$ T cells in tumors of p38i-treated mice compared to the untreated counterparts (Fig. 4E–F). These data indicated that blockade of p38 increased tumor influx by $CD8^+$ T cells.

We further explored the significance of the CD163 and CD8A markers in BC by analyzing expression data using the *Oncomine* tool. Analysis of the BC stroma dataset [32] showed a significant increase in the level of both markers in the BC-associated stroma compared to the normal breast stroma (Suppl. Fig. 4A), although disease recurrence was associated with a lower level of CD8A and a higher level of CD163 (Suppl. Fig. 4B). We hypothesized that

the expression ratio of CD163 and CD8A may serve as a better prognostic indicator of patient survival. This hypothesis was tested in the context of recurrence-free survival (RFS) in BC patients (n=5,143) using an online tool for a Kaplan-Meier estimator [29]. We found a significant association of a high CD163/CD8A expression ratio with disease recurrence (Fig. 4G). Then, the CD163/CD8A ratio was examined in the context of metastasis-free survival using a dataset of 295 BC patients [30] and a prognostic *PROGgene V2* tool [31] (Suppl. Fig. 4C). The data showed that a high CD8A/CD163 ratio correlates with a better prognosis for disease recurrence and MFS. Thus, p38 blockade enhanced tumor infiltration by $CD8^+$ T cells, while reducing the influx of pro-tumor $CD163^+$ TAMs, suggesting a novel strategy to enhance the tumor influx of $CD8^+$ T cells for an improved clinical outcome.

Depletion of granulocytes mimics the response to p38i.

Our data suggested that p38 facilitates the expansion and mobilization of PMN-MDSCs and TAMs, which have been linked to the promotion of metastasis and tumor angiogenesis [10–12]. Thus, we examined whether depletion of PMN-MDSCs recapitulate the response to p38i as an approach to provide further evidence of a non-cell-autonomous mechanism. We performed the experiment as described in Fig. 2, but this time in TB-mice received intraperitoneal (i.p.) injections of anti-Ly6G antibodies to deplete granulocytes, including PMN-MDSCs. Assessment of peripheral blood indicated that anti-Ly6G treatment effectively reduced granulocytes in the circulation, with minimal effects on monocytes (Suppl. Fig. 4D). Treatment with anti-Ly6G also reduced tumor volume at day14 (Fig. 5A–B). Notably, the IHC data revealed a reduction in tumor vasculature and infiltration of $CD163^+$ macrophages, whereas the treatment enhanced tumor infiltration by $CD8^+$ T cells (Fig. 5C). Consistent with these data, prior work indicated that MDSCs subvert macrophages toward an M2-type response in the 4T1 tumor model [47]. Assessment of the lungs and liver showed that the treatment effectively reduced $Ly6G^+$ cells in these tissues (Fig. 5D). Together, these data indicate that depletion of PMN-MDSCs mimics the response to systemic p38 blockade.

p38 controls a tumor-immune crosstalk by regulating tumor-secreted factors acting on myeloid cells

Our findings suggested that p38 regulates the mobilization of pro-tumor myeloid populations, although the mechanisms remained unclear. One hypothesis is that systemic p38 blockade may have a direct effect on generation of the myeloid populations. We tested this hypothesis by assessing the impact of p38i on the generation of immune suppressive MDSCs using a bone marrow culture system *in vitro* [28]. Treatment with p38i did not reduce the generation of either monocytic or granulocytic MDSC populations and did not affect their immune suppressive capacity (Suppl. Fig. 5).

Based on the genetic model (Fig. 5D), we explored the notion that p38 may act in a non-cell-autonomous fashion by controlling the expression of tumor- or stromal-derived chemokines which, in turn, influence the recruitment of pro-tumor myeloid populations to the TME. To that end, we examined whether myeloid populations within the metastatic lung TME expressed chemokine/cytokine receptors for the corresponding ligands produced by the tumor cells. Gene expression profiles of the lungs from tumor-free versus 4T1 TB-mice [33]

showed a significant increase in myeloid cell markers, i.e. S100A8, S100A9, and Stfa2l1 (Fig. 6A), which are associated with chemotactic activity and cancer progression [48]. To validate this finding, we examined expression of myeloid markers in the lungs of control, TB-mice and p38i-treated TB-mice from the study described in Fig. 2. Levels of myeloid markers were significantly increased in TB-mice, while p38i significantly decreased this response (Suppl. Fig. 4E). Importantly, metadata showed that the cytokine and chemokine receptors are among the top elevated genes in the lungs of TB-mice (Fig. 6A). MDSCs infiltrating 4T1 tumors also expressed elevated levels of these aforementioned markers [49].

Next, we asked whether inactivation of p38 diminished the production of tumor-derived factors, focusing on chemokines. Here, we utilized MDA-MB-231 cells expressing dnp38 that inhibited tumor infiltration by TAMs (Fig. 4D). Secretome analysis using the Luminex system detected 15 chemokines and cytokines of 41 tested analytes at biologically relevant concentrations, and these factors were downregulated in dnp38 cells (Fig. 6B). Remarkably, the receptors for the five top regulated factors (CXCL1, CCL2, CCL5, CSF2, and CSF3) were also elevated in the lungs of TB-mice (Fig. 6A–B). Intriguingly, prior research implicated the ligand-receptor pairs CXCL1-CXCR2, CCL2-CCR2, CSF2-CSF2RB, and CCL5-CCR1 in the mobilization of myeloid populations including TAMs and MDSCs [15, 50]. Further, we found that the expression of Cxcr2 and Csf2rb receptors was significantly increased in the lungs of TB-mice, while their levels were reduced in p38i-treated TB-mice (Suppl. Fig. 4E). Next, we examined CCL2 levels in tumor and stromal cells, as both cell types express this cytokine [15]. Quantitative RT-PCR showed a significant reduction of CCL2 mRNA levels by p38i in both cell types (Fig. 6C). Furthermore, ELISA showed that p38i reduced CCL2/MCP-1 levels by nearly 3-fold in 4T1 cells and by 2-fold in tumors (Suppl. Fig. 4F–G). Together, these data indicated that p38 regulates TME-produced secretory factors, while their cognate receptors are expressed on pro-tumor myeloid populations such as TAMs and MDSCs.

To explore the relevance of these observations to human BC, we examined the expression of the myeloid-related genes in the TCGA datasets. Genomic data revealed elevated levels of the ligands, their receptors and myeloid cell markers in TNBC/basal carcinomas (Fig. 6D). Notably, TNBC also expressed high levels of mesenchymal/EMT markers. Further, the Kaplan-Meier data showed a significant inverse association of high mRNA levels of CCR1 and a myeloid marker S100A8 with recurrence-free survival in BC patients (Fig. 6E). Together, these data suggested that p38 in carcinoma and stromal cells regulates the expression of cytokines and chemokines that facilitate the mobilization of pro-tumor myeloid populations (Fig. 6F).

DISCUSSION

Metastatic breast cancer (MBC) is a life-threatening stage of disease that urgently requires more effective therapies. While tumor progression to metastasis is a highly complex process, it is becoming clear that successful metastasis reflects not only cell-autonomous, but also cell-non-autonomous mechanisms [5, 51]. In this study, we found that a clinically relevant anti-p38 agent inhibits metastasis of breast cancer to the lungs by reducing tumor-induced mobilization of myeloid populations. Our data suggest that p38 acts in tumor and stromal

cells by regulating the expression of cytokines and chemokines, which facilitate the mobilization of pro-tumor myeloid populations. Overall, we demonstrated that: *1)* administration of a pharmacologic p38 inhibitor (p38i) diminished TNBC growth, angiogenesis, and metastasis concomitant with a dramatic reduction in TAMs and MDSCs within the TME; *2)* depletion of MDSCs, which was accompanied by a reduction in TAMs, recapitulated the anti-metastatic effects of p38 blockade; reciprocally, this led to an increase in intratumoral $CD8^+$ T cells; *3)* genetic or pharmacological blockade of p38 reduced the expression of tumor- and stromal-derived chemokines known to facilitate the recruitment of pro-tumor myeloid populations; and *4)* an elevated CD8/TAM ratio was associated with increased breast cancer patient survival, indicating that p38 blockade may be a novel strategy to alter this ratio to improve clinical outcome. Thus, our study indicates that p38 contributes to MBC *via* cell non-autonomous myeloid-dependent mechanisms.

Our work revealed an unrecognized pro-tumor p38 activity mediated through the mobilization of myeloid populations, such as MDSCs and TAMs. MDSCs comprise heterogeneous populations of pathologically activated immature myeloid cells, which accumulate during disease progression and suppress immune responses, while facilitating metastasis [37]. Expansion of MDSCs is well-documented in multiple preclinical tumor models, including the 4T1 mouse mammary carcinoma and the MDA-MB-231 human TNBC cell line models [10, 13, 14, 33, 35, 47]. Our data demonstrate that inhibition of p38 blocks the expansion of MDSCs and their mobilization to the lungs and liver, while reducing tumor infiltration by TAMs. Remarkably, inactivation of p38 in cancer cells by a genetic approach phenocopied the response to the pharmacological inhibitor with respect to a reduction in TAMs and inhibition of tumor angiogenesis and lung metastasis. These data link the pro-tumor function of p38 to the control of expansion and mobilization of pro-tumor myeloid populations.

MDSCs contribute to the formation of the pre-metastatic niche, facilitating spread to the lungs and liver [11, 33]. Here, blockade of p38 reduced the expansion of PMN-MDSCs in the spleen and mobilization of PMN-MDSCs to the lungs and liver. The presence of cancer stimulated the expansion of the red-pulp zones in the spleen, increasing MK cells and PMN-MDSCs. While this tumor-induced extramedullary myelopoiesis is well-characterized [13, 14, 33, 35], the current study revealed p38 as a previously unidentified and important mediator of this response. Our data showed that blockade of p38 reduced tumor-driven expansion of the splenic myeloid compartment and the production of MK cells. Extramedullary myelopoiesis or hematopoiesis (EMH) may occur in the spleen, liver and other organs outside of the bone marrow, particularly in cases of cancer and acute infections [41, 52, 53]. Our data provide an exciting prospect to restrain EMH, a potential source of these myeloid populations, in both acute and chronic pathologies using the anti-p38-class of agents.

Our data suggest that p38 regulates communication between the tumor and host immune cells. We found that p38 controls the expression of an array of cytokines and chemokines (e.g., CCL2, CXCL1, GM-CSF, and G-CSF) by tumor cells and MSCs, while myeloid cells express their corresponding cognate receptors. The data on genetic inactivation of p38 in BC cells and the TCGA data further support this model. Prior studies have shown that the

CXCL1-CXCR2 pair promotes the accumulation of PMN-MDSCs [9], while the CCL2-CCR2 pair regulates tumor infiltration by TAMs [15], as well as PMN-MDSCs [54]. Evidence also implicates G-CSF and GM-CSF in the mobilization of myeloid populations including PMN-MDSCs [13, 33, 55]. While p38 blockade *in vivo* could diminish the production of MDSCs, we did not observe this effect *in vitro* using a bone marrow culture system. This suggests that p38 may impact MDSC biology post-development, which is consistent with prior research showing that p38 blockade may impact the migration and release of cytokines by myeloid cells [56]. Thus, p38 may mediate the release of cytokines in multiple cell types in the breast TME, contributing to the mobilization of such pro-metastatic myeloid populations. Future studies are warranted, however, to test these hypotheses in detail.

Of the four p38 isoforms, p38-α isoform is expressed at high levels by human breast (MDA-MB-231) and mouse (4T1) mammary carcinoma cell lines [17–20]. The p38 inhibitor used in the study (Ralimetinib) selectively inhibits p38-α/β isoforms while the inhibitory activity towards γ/δ isoforms is negligible [24, 25, 57]. In addition, genetic inactivation of p38-α results in the inhibition of phosphorylation of the p38 effectors such as MK2, HSP27, and CREB/ATF1 [17, 18, 20], as well as reduces metastasis [17, 18, 20, 58]. Nonetheless, recent data suggest a more complex role of p38 isoforms in the regulation of inflammatory pathways related to cancer. Notably, inhibition of p38-α may trigger activation of p38-δ, indicating a more complex interdependence of the kinase isoforms [59]. Thus, while our study suggests a link of p38-α/β isoforms to tumor-induced myeloid cell mobilization, these and other reported findings reinforce the complexity of the p38-mediated networks in tumor progression and metastasis.

A strong anti-angiogenic activity of p38i is consistent with the effect of genetic inactivation of p38 in human BC cells [19]. Prior work showed that p38 regulates the production of vascular growth factors by the tumor-stromal crosstalk in the TME [19]. Our study suggests that p38 also contributes to tumor angiogenesis through a mechanism involving TAMs and PMN-MDSCs. Our data show that depletion of PMN-MDSCs impedes tumor vasculature and tumor infiltration by $CD163^+$ (M2-type) TAMs, which is consistent with prior work linking MDSCs to the subsequent regulation of an M2-type TAM response [47]. Thus, the p38-MDSC pathway may represent a potential target for anti-angiogenic therapy, providing an alternative strategy. Inhibition of p38 may also improve the efficacy of current anti-angiogenics, as TAMs and MDSCs contribute to the resistance to anti-angiogenics targeting the VEGF pathway [60].

The clinical significance of the p38-myeloid mechanism is further supported by genomic BC data. Metadata revealed high levels of p38-dependent ligands, their receptors and MDSC markers in TNBC/basal carcinomas. Further, the p38i agent reduced tumor infiltration by $CD163^+$ TAMs, while increasing the presence of $CD8^+$ T cells in the tumor. Conversely, metadata for the expression ratio of CD163/CD8A in BC suggested a correlation with worse disease relapse, and this was statistically significant.

In summary, this work implicates the p38 kinase in the control of tumor-induced expansion and mobilization of pro-tumor myeloid populations. This response supports breast cancer angiogenesis and metastasis, providing a novel therapeutic target in MBC. Notably, our

study made use of p38 blockade as a monotherapy mainly to focus on its mode-of-action, but it likely will have greater utility in combination with standard-of-care or immune-targeted therapies, such as immune checkpoint blockade which has led to durable responses, but only in subsets of patients. In those settings, p38 blockade represents a new paradigm to lessen pro-angiogenic or myeloid-mediated pro-tumorigenic mechanisms that might interfere with optimal combinatorial therapeutic efficacy.

Supplementary Material

Refer to Web version on PubMed Central for supplementary material.

ACKNOWLEDGEMENTS

We gratefully acknowledge the generous help from Flow and Image Cytometry Facility, the Pathology Resource Network, Preclinical Imaging Services, and Laboratory Animal Resource (LAR). We thank Dr. Elizabeth Repasky for providing reagents; Rebecca Walden for help in the study; Dr. Spernyak and his team for assistance in Bioluminescence imaging.

FINANCIAL SUPPORT

Department of Defense BCRP Program BC151886 (to AVB), Roswell Park Alliance Foundation (to AVB), NIH R01CA172105 (to SIA), NIH training grant T32CA085183 (to SHC) and a pre-doctoral fellowship F31CA228396 (to SHC), Metastatic Breast Cancer METAvivor foundation (to AVB and SIA), and in part by NIH R25CA181003 (to AM) and the Roswell Park Comprehensive Cancer Center Support Grant, P30CA016056

LIST OF ABBREVIATIONS

HSP27	heat-shock protein 27
MAPK	mitogen-activated protein kinase
MDSC	Myeloid-derived suppressor cells
MMP9	matrix metalloproteinase 9
MSC	Mesenchymal stromal cells
TAK1	TGF-beta activated kinase 1
TGF-β	transforming growth factor beta
TNBC	triple-negative breast cancer
TNF	Tumor necrosis factor
VEGFA	vascular endothelial growth factor A

REFERENCES

1. Siegel RL, Miller KD, Jemal A. Cancer statistics, 2018. CA: A Cancer Journal for Clinicians 2018;68: 7–30. [PubMed: 29313949]
2. Cortazar P, Zhang L, Untch M, Mehta K, Costantino JP, Wolmark N, Bonnefoi H, Cameron D, Gianni L, Valagussa P, Swain SM, Prowell T, et al. Pathological complete response and long-term clinical benefit in breast cancer: the CTNeoBC pooled analysis. The Lancet 2014;384: 164–72.

3. Zeichner SB, Terawaki H, Gogineni K. A Review of Systemic Treatment in Metastatic Triple-Negative Breast Cancer. Breast Cancer : Basic and Clinical *Research* 2016;10: 25–36. [PubMed: 27042088]
4. Saleh SMI, Bertos N, Gruosso T, Gigoux M, Souleimanova M, Zhao H, Omeroglu A, Hallett MT, Park M. Identification of Interacting Stromal Axes in Triple-Negative Breast Cancer. Cancer Research 2017;77: 4673. [PubMed: 28652250]
5. McAllister SS, Weinberg RA. The tumour-induced systemic environment as a critical regulator of cancer progression and metastasis. Nature Cell Biology 2014;16: 717. [PubMed: 25082194]
6. Limoge M, Safina A, Beattie A, Kapus L, Truskinovsky AM, Bakin AV. Tumor-fibroblast interactions stimulate tumor vascularization by enhancing cytokine-driven production of MMP9 by tumor cells. Oncotarget 2017;8: 35592–608. [PubMed: 28423685]
7. Rajaram M, Li J, Egeblad M, Powers RS. System-Wide Analysis Reveals a Complex Network of Tumor-Fibroblast Interactions Involved in Tumorigenicity. PLoS Genet 2013;9: e1003789. [PubMed: 24068959]
8. Liao D, Luo Y, Markowitz D, Xiang R, Reisfeld RA. Cancer Associated Fibroblasts Promote Tumor Growth and Metastasis by Modulating the Tumor Immune Microenvironment in a 4T1 Murine Breast Cancer Model. *PLoS ONE* 2009;4: e7965. [PubMed: 19956757]
9. Kumar V, Donthireddy L, Marvel D, Condamine T, Wang F, Lavilla-Alonso S, Hashimoto A, Vonteddu P, Behera R, Goins MA, Mulligan C, Nam B, et al. Cancer-Associated Fibroblasts Neutralize the Anti-tumor Effect of CSF1 Receptor Blockade by Inducing PMN-MDSC Infiltration of Tumors. Cancer Cell 2017;32: 654–68.e5. [PubMed: 29136508]
10. Ouzounova M, Lee E, Piranlioglu R, El Andaloussi A, Kolhe R, Demirci MF, Marasco D, Asm I, Chadli A, Hassan KA, Thangaraju M, Zhou G, et al. Monocytic and granulocytic myeloid derived suppressor cells differentially regulate spatiotemporal tumour plasticity during metastatic cascade. Nature Communications 2017;8: 14979.
11. Tabaries S, Ouellet V, Hsu BE, Annis MG, Rose AA, Meunier L, Carmona E, Tam CE, Mes-Masson AM, Siegel PM. Granulocytic immune infiltrates are essential for the efficient formation of breast cancer liver metastases. Breast cancer research : BCR 2015;17: 45. [PubMed: 25882816]
12. Peinado H, Zhang H, Matei IR, Costa-Silva B, Hoshino A, Rodrigues G, Psaila B, Kaplan RN, Bromberg JF, Kang Y, Bissell MJ, Cox TR, et al. Pre-metastatic niches: organ-specific homes for metastases. Nat Rev Cancer 2017;17: 302–17. [PubMed: 28303905]
13. Waight JD, Hu Q, Miller A, Liu S, Abrams SI. Tumor-Derived G-CSF Facilitates Neoplastic Growth through a Granulocytic Myeloid-Derived Suppressor Cell-Dependent Mechanism. PLoS ONE 2011;6: e27690. [PubMed: 22110722]
14. Youn J-I, Nagaraj S, Collazo M, Gabrilovich DI. Subsets of Myeloid-Derived Suppressor Cells in Tumor-Bearing Mice. The Journal of Immunology 2008;181: 5791. [PubMed: 18832739]
15. Qian B-Z, Li J, Zhang H, Kitamura T, Zhang J, Campion LR, Kaiser EA, Snyder LA, Pollard JW. CCL2 recruits inflammatory monocytes to facilitate breast-tumour metastasis. Nature 2011;475: 222. [PubMed: 21654748]
16. Brichkina A, Bertero T, Loh HM, Nguyen NTM, Emelyanov A, Rigade S, Ilie M, Hofman P, Gaggioli C, Bulavin DV. p38MAPK builds a hyaluronan cancer niche to drive lung tumorigenesis. Genes & Development 2016;30: 2623–36. [PubMed: 28007785]
17. Bakin AV, Rinehart C, Tomlinson AK, Arteaga CL. p38 mitogen-activated protein kinase is required for TGF{beta}-mediated fibroblastic transdifferentiation and cell migration. J Cell Sci 2002;115: 3193–206. [PubMed: 12118074]
18. Wu X, Zhang W, Font-Burgada J, Palmer T, Hamil AS, Biswas SK, Poidinger M, Borcherding N, Xie Q, Ellies LG, Lytle NK, Wu L-W, et al. Ubiquitin-conjugating enzyme Ubc13 controls breast cancer metastasis through a TAK1-p38 MAP kinase cascade. Proceedings of the National Academy of Sciences of the United States of America 2014;111: 13870–5. [PubMed: 25189770]
19. Limoge M, Safina A, Truskinovsky AM, Aljahdali I, Zonneville J, Gruevski A, Arteaga CL, Bakin AV. Tumor p38MAPK signaling enhances breast carcinoma vascularization and growth by promoting expression and deposition of pro-tumorigenic factors. Oncotarget 2017: 1–13.

20. Iriondo O, Liu Y, Lee G, Elhodaky M, Jimenez C, Li L, Lang J, Wang P, Yu M. TAK1 mediates microenvironment-triggered autocrine signals and promotes triple-negative breast cancer lung metastasis. Nat Commun 2018;9: 1994. [PubMed: 29777109]
21. Davidson B, Konstantinovsky S, Kleinberg L, Nguyen MTP, Bassarova A, Kvalheim G, Nesland JM, Reich R. The mitogen-activated protein kinases (MAPK) p38 and JNK are markers of tumor progression in breast carcinoma. Gynecologic Oncology 2006;102: 453–61. [PubMed: 16494928]
22. Wagner EF, Nebreda AR. Signal integration by JNK and p38 MAPK pathways in cancer development. Nat Rev Cancer 2009;9: 537–49. [PubMed: 19629069]
23. Alspach E, Flanagan KC, Luo X, Ruhland MK, Huang H, Pazolli E, Donlin MJ, Marsh T, Piwnica-Worms D, Monahan J, Novack DV, McAllister SS, et al. p38MAPK Plays a Crucial Role in Stromal-Mediated Tumorigenesis. Cancer Discovery 2014;4: 716. [PubMed: 24670723]
24. Norman P Investigational p38 inhibitors for the treatment of chronic obstructive pulmonary disease. Expert Opinion on Investigational Drugs 2015;24: 383–92. [PubMed: 25599809]
25. Campbell RM, Anderson BD, Brooks NA, Brooks HB, Chan EM, De Dios A, Gilmour R, Graff JR, Jambrina E, Mader M, McCann D, Na S, et al. Characterization of LY2228820 Dimesylate, a Potent and Selective Inhibitor of p38 MAPK with Antitumor Activity. Molecular Cancer Therapeutics 2014;13: 364. [PubMed: 24356814]
26. Weidner N, Semple J, Welch W, Folkman J. Tumor angiogenesis and metastasis--correlation in invasive breast carcinoma. N Engl J Med 1991;324: 1–8.
27. Liang L, Fan Y, Cheng J, Cheng D, Zhao Y, Cao B, Ma L, An L, Jia W, Su X, Yang J, Zhang H. TAK1 ubiquitination regulates doxorubicin-induced NF-κB activation. Cellular Signalling 2013;25: 247–54. [PubMed: 22981905]
28. Netherby CS, Messmer MN, Burkard-Mandel L, Colligan S, Miller A, Cortes Gomez E, Wang J, Nemeth MJ, Abrams SI. The Granulocyte Progenitor Stage Is a Key Target of IRF8-Mediated Regulation of Myeloid-Derived Suppressor Cell Production. The Journal of Immunology 2017;198: 4129. [PubMed: 28356386]
29. Gyorffy B, Lanczky A, Eklund AC, Denkert C, Budczies J, Li Q, Szallasi Z. An online survival analysis tool to rapidly assess the effect of 22,277 genes on breast cancer prognosis using microarray data of 1,809 patients. Breast Cancer Res Treat 2010;123: 725–31. [PubMed: 20020197]
30. Drukker CA, van Tinteren H, Schmidt MK, Rutgers EJT, Bernards R, van de Vijver MJ, van't Veer LJ. Long-term impact of the 70-gene signature on breast cancer outcome. Breast Cancer Research and Treatment 2014;143: 587–92. [PubMed: 24445566]
31. Goswami CP, Nakshatri H. PROGgene: gene expression based survival analysis web application for multiple cancers. Journal of Clinical Bioinformatics 2013;3: 22-. [PubMed: 24165311]
32. Finak G, Bertos N, Pepin F, Sadekova S, Souleimanova M, Zhao H, Chen H, Omeroglu G, Meterissian S, Omeroglu A, Hallett M, Park M. Stromal gene expression predicts clinical outcome in breast cancer. Nature Medicine 2008;14: 518–27.
33. Kowanetz M, Wu X, Lee J, Tan M, Hagenbeek T, Qu X, Yu L, Ross J, Korsisaari N, Cao T, Bou-Reslan H, Kallop D, et al. Granulocyte-colony stimulating factor promotes lung metastasis through mobilization of Ly6G+Ly6C+ granulocytes. Proceedings of the National Academy of Sciences 2010;107: 21248.
34. Muraoka RS, Dumont N, Ritter CA, Dugger TC, Brantley DM, Chen J, Easterly E, Roebuck LR, Ryan S, Gotwals PJ, Koteliansky V, Arteaga CL. Blockade of TGF-beta inhibits mammary tumor cell viability, migration, and metastases. J Clin Invest 2002;109: 1551–9. [PubMed: 12070302]
35. duPre SA, Hunter KW. Murine mammary carcinoma 4T1 induces a leukemoid reaction with splenomegaly: Association with tumor-derived growth factors. Experimental and Molecular Pathology 2007;82: 12–24. [PubMed: 16919266]
36. Pulaski BA, Ostrand-Rosenberg S. Mouse 4T1 Breast Tumor Model Current Protocols in Immunologyed.: John Wiley & Sons, Inc, 2001.
37. Bronte V, Brandau S, Chen S-H, Colombo MP, Frey AB, Greten TF, Mandruzzato S, Murray PJ, Ochoa A, Ostrand-Rosenberg S, Rodriguez PC, Sica A, et al. Recommendations for myeloid-derived suppressor cell nomenclature and characterization standards. Nature Communications 2016;7: 12150.

38. Bunt SK, Sinha P, Clements VK, Leips J, Ostrand-Rosenberg S. Inflammation Induces Myeloid-Derived Suppressor Cells that Facilitate Tumor Progression. The Journal of Immunology 2006;176: 284. [PubMed: 16365420]
39. Stewart TJ, Liewehr DJ, Steinberg SM, Greeneltch KM, Abrams SI. Modulating the Expression of IFN Regulatory Factor 8 Alters the Protumorigenic Behavior of CD11b⁺Gr-1⁺ Myeloid Cells. The Journal of Immunology 2009;183: 117. [PubMed: 19542426]
40. Wu C, Ning H, Liu M, Lin J, Luo S, Zhu W, Xu J, Wu W-C, Liang J, Shao C-K, Ren J, Wei B, et al. Spleen mediates a distinct hematopoietic progenitor response supporting tumor-promoting myelopoiesis. The Journal of Clinical Investigation 2018;128: 3425–38. [PubMed: 29771686]
41. Zhao L, He R, Long H, Guo B, Jia Q, Qin D, Liu SQ, Wang Z, Xiang T, Zhang J, Tan Y, Huang J, et al. Late-stage tumors induce anemia and immunosuppressive extramedullary erythroid progenitor cells. Nat Med 2018;24: 1536–44. [PubMed: 30297899]
42. Elmore SA. Enhanced Histopathology of the Spleen. Toxicologic pathology 2006;34: 648–55. [PubMed: 17067950]
43. Tiainen S, Tumelius R, Rilla K, Hämäläinen K, Tammi M, Tammi R, Kosma V-M, Oikari S, Auvinen P. High numbers of macrophages, especially M2-like (CD163-positive), correlate with hyaluronan accumulation and poor outcome in breast cancer. Histopathology 2014;66: 873–83.
44. Sousa S, Brion R, Lintunen M, Kronqvist P, Sandholm J, Monkkonen J, Kellokumpu-Lehtinen PL, Lauttia S, Tynninen O, Joensuu H, Heymann D, Maatta JA. Human breast cancer cells educate macrophages toward the M2 activation status. *Breast cancer research* : BCR 2015;17: 101. [PubMed: 26243145]
45. Brown JM, Recht L, Strober S. The Promise of Targeting Macrophages in Cancer Therapy. Clinical Cancer Research 2017;23: 3241. [PubMed: 28341752]
46. Ku AW, Muhitch JB, Powers CA, Diehl M, Kim M, Fisher DT, Sharda AP, Clements VK, O'Loughlin K, Minderman H, Messmer MN, Ma J, et al. Tumor-induced MDSC act via remote control to inhibit L-selectin-dependent adaptive immunity in lymph nodes. eLife 2016;5.
47. Sinha P, Clements VK, Bunt SK, Albelda SM, Ostrand-Rosenberg S. Cross-talk between myeloid-derived suppressor cells and macrophages subverts tumor immunity toward a type 2 response. J Immunol 2007;179: 977–83. [PubMed: 17617589]
48. Ryckman C, Vandal K, Rouleau P, Talbot M, Tessier PA. Proinflammatory Activities of S100: Proteins S100A8, S100A9, and S100A8/A9 Induce Neutrophil Chemotaxis and Adhesion. The Journal of Immunology 2003;170: 3233. [PubMed: 12626582]
49. Elpek KG, Cremasco V, Shen H, Harvey CJ, Wucherpfennig KW, Goldstein DR, Monach PA, Turley SJ. The Tumor Microenvironment Shapes Lineage, Transcriptional, and Functional Diversity of Infiltrating Myeloid Cells. Cancer Immunology Research 2014;2: 655. [PubMed: 24801837]
50. Zhang Y, Lv D, Kim H-J, Kurt RA, Bu W, Li Y, Ma X. A novel role of hematopoietic CCL5 in promoting triple-negative mammary tumor progression by regulating generation of myeloid-derived suppressor cells. Cell Research 2012;23: 394. [PubMed: 23266888]
51. Binnewies M, Roberts EW, Kersten K, Chan V, Fearon DF, Merad M, Coussens LM, Gabrilovich DI, Ostrand-Rosenberg S, Hedrick CC, Vonderheide RH, Pittet MJ, et al. Understanding the tumor immune microenvironment (TIME) for effective therapy. Nat Med 2018;24: 541–50. [PubMed: 29686425]
52. Inra CN, Zhou BO, Acar M, Murphy MM, Richardson J, Zhao Z, Morrison SJ. A perisinusoidal niche for extramedullary haematopoiesis in the spleen. Nature 2015;527: 466. [PubMed: 26570997]
53. Bowling MR, Cauthen CG, Perry CD, Patel NP, Bergman S, Link KM, Sane AC, Conforti JF. Pulmonary extramedullary hematopoiesis. Journal of thoracic imaging 2008;23: 138–41. [PubMed: 18520574]
54. Chun E, Lavoie S, Michaud M, Gallini Carey A, Kim J, Soucy G, Odze R, Glickman Jonathan N, Garrett Wendy S. CCL2 Promotes Colorectal Carcinogenesis by Enhancing Polymorphonuclear Myeloid-Derived Suppressor Cell Population and Function. Cell Reports 2015;12: 244–57. [PubMed: 26146082]

55. Mehta HM, Malandra M, Corey SJ. G-CSF and GM-CSF in Neutropenia. The Journal of Immunology 2015;195: 1341. [PubMed: 26254266]

56. Nick JA, Young SK, Brown KK, Avdi NJ, Arndt PG, Suratt BT, Janes MS, Henson PM, Worthen GS. Role of p38 Mitogen-Activated Protein Kinase in a Murine Model of Pulmonary Inflammation. The Journal of Immunology 2000;164: 2151. [PubMed: 10657669]

57. Tate CM, Blosser W, Wyss L, Evans G, Xue Q, Pan Y, Stancato L. LY2228820 Dimesylate, a Selective Inhibitor of p38 Mitogen-activated Protein Kinase, Reduces Angiogenic Endothelial Cord Formation in Vitro and in Vivo. The Journal of Biological Chemistry 2013;288: 6743–53. [PubMed: 23335506]

58. Junttila MR, Ala-aho R, Jokilehto T, Peltonen J, Kallajoki M, Grenman R, Jaakkola P, Westermarck J, Kähäri VM. p38α and p38δ mitogen-activated protein kinase isoforms regulate invasion and growth of head and neck squamous carcinoma cells. Oncogene 2007;26: 5267. [PubMed: 17334397]

59. Matesanz N, Nikolic I, Leiva M, Pulgarin-Alfaro M, Santamans AM, Bernardo E, Mora A, Herrera-Melle L, Rodriguez E, Beiroa D, Caballero A, Martin-Garcia E, et al. p38alpha blocks brown adipose tissue thermogenesis through p38delta inhibition. PLoS biology 2018;16: e2004455. [PubMed: 29979672]

60. Bergers G, Hanahan D. Modes of resistance to anti-angiogenic therapy. Nature Reviews Cancer 2008;8: 592–603. [PubMed: 18650835]

SIGNIFICANCE

The study discovered that a clinically relevant anti-p38 agent inhibits breast cancer metastasis to the lungs by impeding the recruitment of pro-tumor myeloid cells, suggesting that targeting this pathway has important implications for cancer immunotherapy.

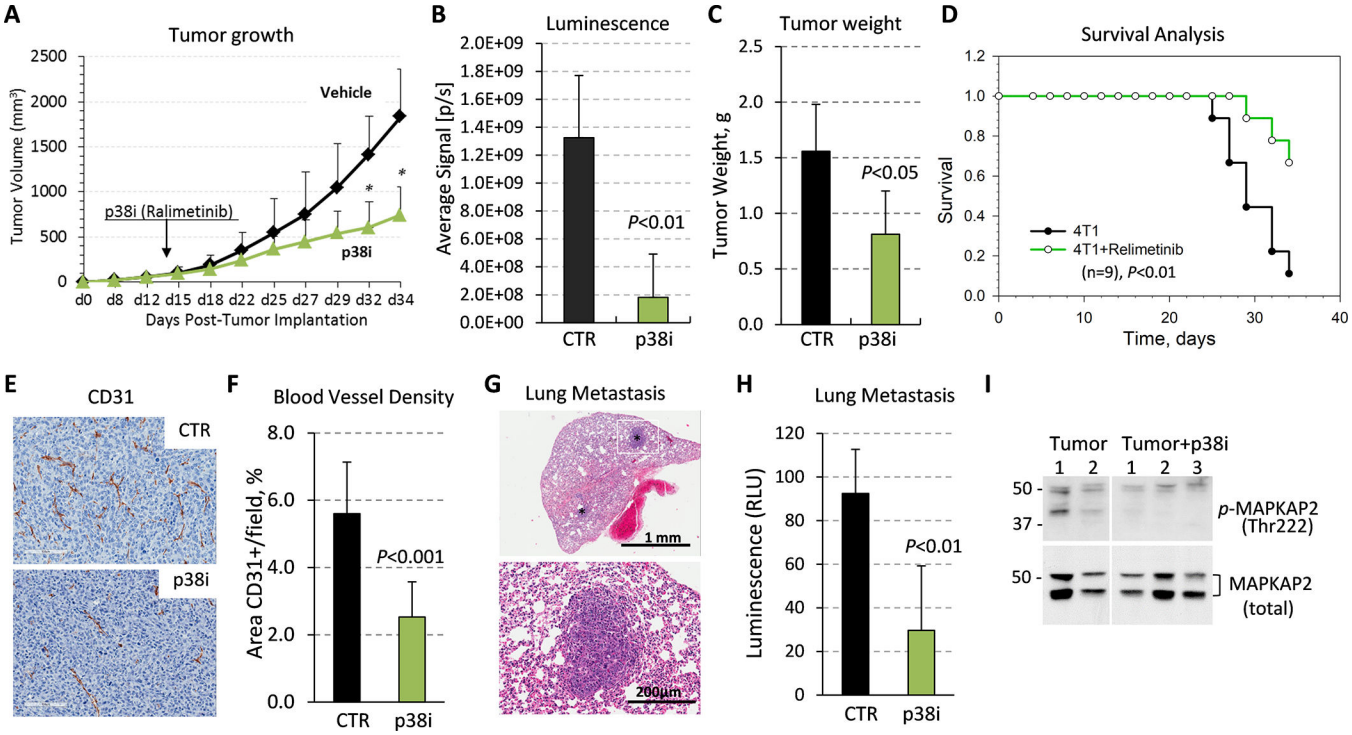

Figure 1. Tumor growth and metastasis are reduced by systemic treatment with a p38 inhibitor.

(**A**) 4T1-Luc mammary carcinoma cells (50,000) were orthotopically implanted into female BALB/c female 6-week old mice (9 mice per group). Starting on day 14 post-tumor implantation, when the tumor size reached ~100mm^3, mice were treated by daily oral gavage with vehicle-control (saline) or p38i (Ralimetinib). (**B**) Quantification of bioluminescence in live animals at day 34. (**C**) Tumor weight at day 34. (**D**) Survival was evaluated using Kaplan-Meier estimator based on time-to-arrive at 1cm3 of tumor size measured in 4T1 tumor-bearing mice in non-treated (4T1) and Ralimetinib-treated groups, (n=9). Comparison was made using the Log-rank test (P<0.01). (**E**) Tumor blood vessels were visualized by anti-CD31 staining, bar=100µm. (**F**) The microvessel density was evaluated on comparable size tumors using CD31-stained sections in six fields for each case (3 tumors/group) and presented as mean area per field (0.2 mm^2). Statistical significance was determined using the two-tailed unpaired *t*-test (*P*<0.05). (**G**) Detection of metastases in H&E-stained lung sections. (**H**) Luminescence activity in whole-cell extracts from the lungs of control or p38i-treated comparable size groups, 3 mice per group. (**I**) Immunoblots of whole tumor extracts from mice bearing 4T1 tumors from the vehicle control and p38i-treated groups.

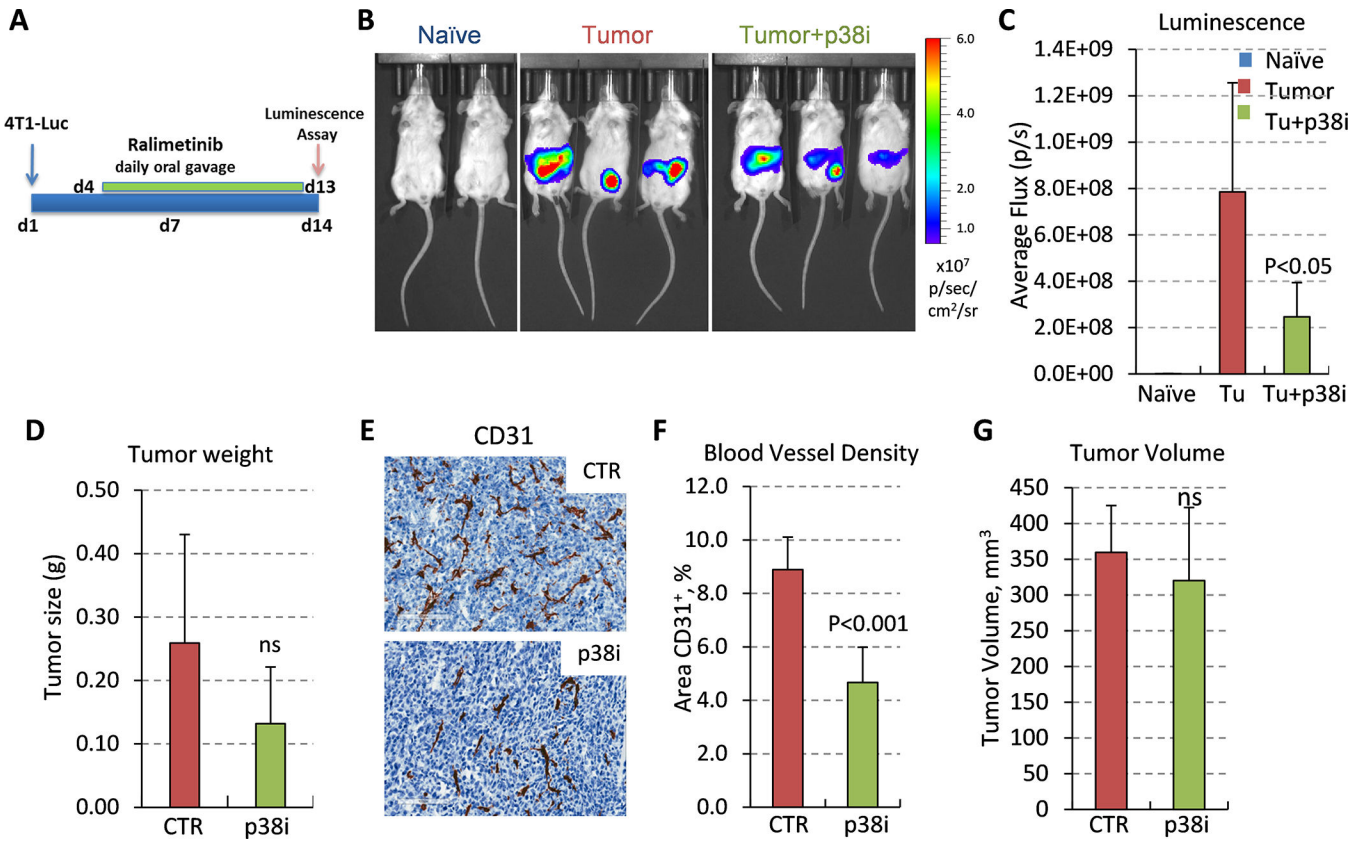

Figure 2. Blockade of p38 kinase reduces angiogenesis at the early tumor growth stage.

(**A**) The study outline: 4T1-Luc mammary carcinoma cells (200,000) were orthotopically implanted into BALB/c female 6-week old mice (9 mice per group). Treatment with p38i/Ralimetinib at 30mg/kg was initiated on day 4 by daily oral gavage. (**B**) Bioluminescence images of tumor-free (naïve), tumor-bearing (tumor), or tumor-bearing and p38i-treated mice. Note the absence of luminescence at the lungs. (**C**) Quantification of bioluminescence in live animals on day 14. (**D**) Tumor weight (median) at day 14 of the study. (**E**) Images of CD31-stained tumor sections from untreated or p38i-treated tumor-bearing mice, bar=100μm. (**F**) Quantification of the microvessel density in CD31-stained sections of comparable-size tumors (**G**), a mean area per field (0.2 mm^2), 6 fields per tumor section, 3 tumors per group. (**G**) Comparison of tumor volumes from untreated and p38i-treated groups. Statistical significance was determined using the two-tailed unpaired *t*-test ($P<0.05$; ns, not significant, P>0.05).

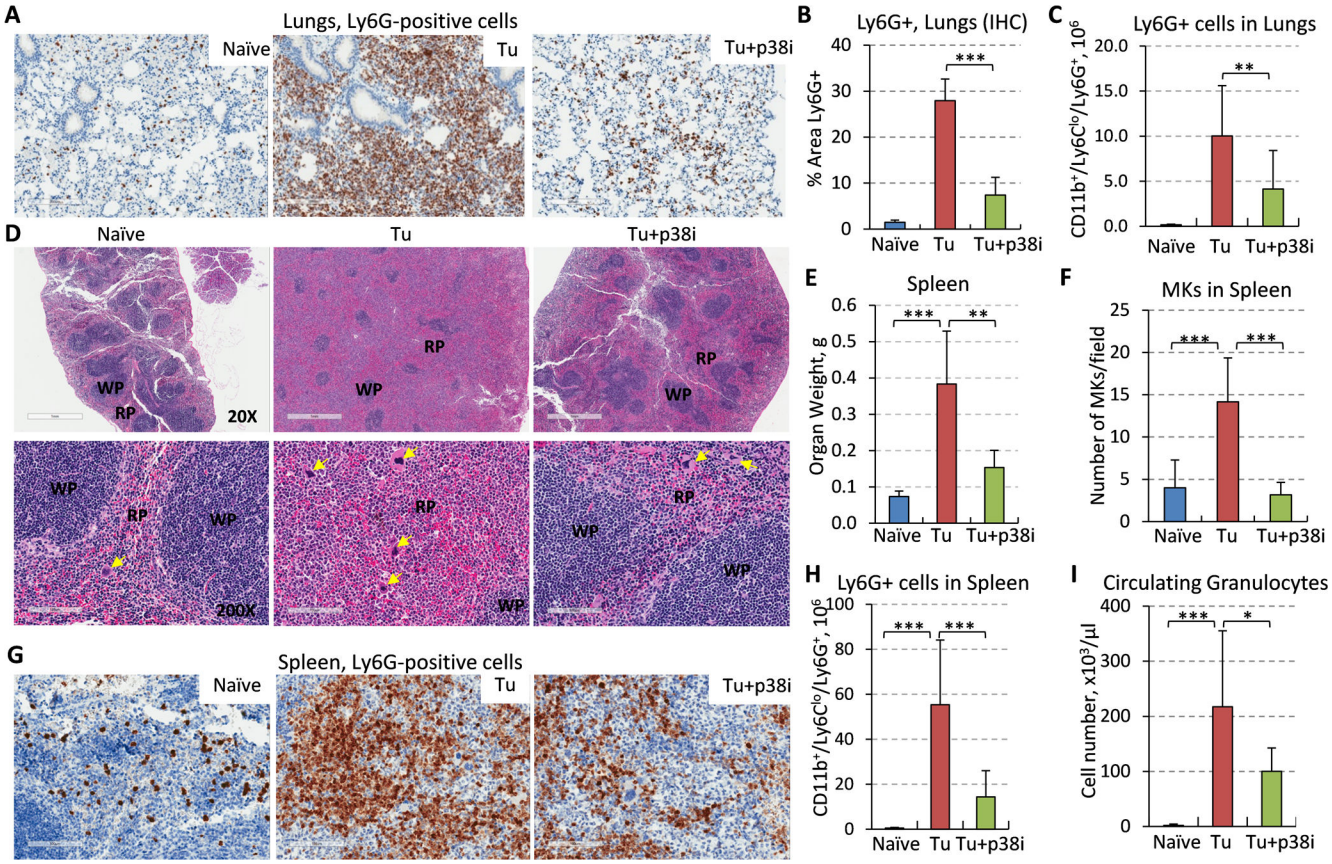

Figure 3. Blockade of p38 reduces accumulation of MDSCs in the lungs and the expansion of PMN-MDSCs and megakaryocytes in the spleen of tumor-bearing mice.

(**A**) Lung tissues from tumor-free (naïve), 4T1-Luc tumor-bearing (Tu) and tumor-bearing mice treated with p38i were stained for Ly6G, a marker of PMN-MDSCs, bar=200µm. (**B**) Quantification of $Ly6G^+$ cells in the lung sections, 3 fields per section, 3 mice per group. (**C**) Flow cytometry analysis of $CD11b^+Ly6C^{lo}Ly6G^+$ cells in whole-lung tissues, 3 mice per group. (**D**) H&E-stained spleen tissues at 20x magnification (top row, bar=1mm), bottom at 200x, bar=100µm. Yellow arrows show megakaryocytes; WP, white pulp; RP, red pulp. Note an increase in the RP and spleen size in tumor-bearing mice compared to tumor-free mice, and their reduction by p38i/Ralimetinib. (**E**) Spleen weights were measured at day 14 of the study, n=5. (**F**) Evaluation of megakaryocytes (MK) in the spleen of tumor-free (naïve), tumor-bearing (Tu), and tumor-bearing treated with p38i (Tu+p38i). (**G**) Spleen sections stained for Ly6G, bar=100µm. (**H**) Flow cytometry data for $CD11b^+Ly6C^{lo}Ly6G^+$ cells in whole-spleen tissue from 3 mice per group. (**I**) Quantification of granulocytes in peripheral blood using complete blood count (CBC) assays. Comparisons were done with material from naïve mice and mice with comparably sized tumors, and statistical significance was determined using the two-tailed unpaired *t*-test (*P<0.05; **P<0.01; ***P<0.001).

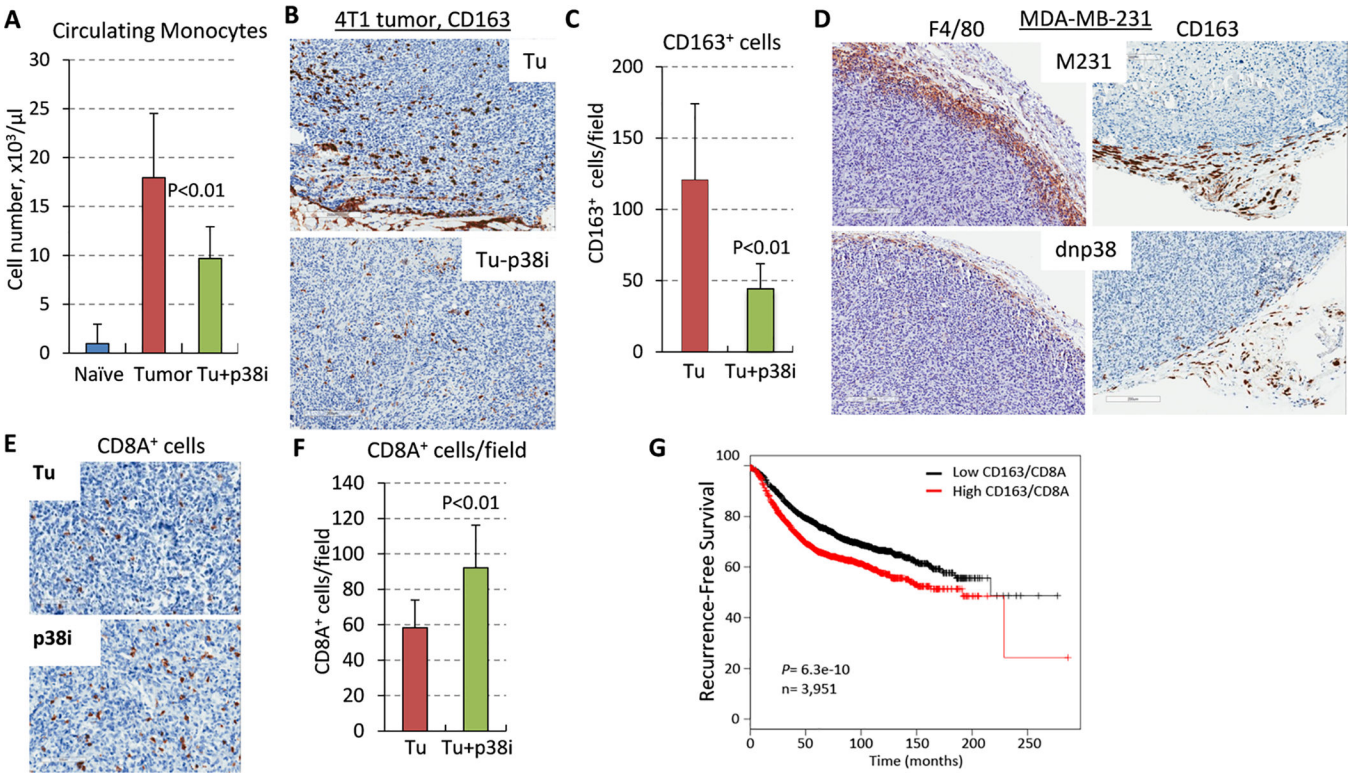

Figure 4. Evaluation of CD163$^+$ macrophages in tumor tissues.

(**A**) Quantification of monocytes in peripheral of tumor-free mice (naïve), tumor-bearing untreated (Tu) or p38i-treated mice by CBC assays at day 14 of the study. (**B**) Images of CD163-stained tumor sections, bar=100µm. (**C**) Quantification of CD163$^+$ cells in tumor tissues, 3 fields/section, 3 sections/group. (**D**) Images of CD163 and F4/80-stained sections of tumor xenografts of MDA-MB-231 human breast cancer cells (empty-vector control and dnp38) in SCID mice, bar=200µm. (**E**) Images of CD8A-stained 4T1-Luc tumor sections, bar=100µm. (**F**) Quantification of CD8A$^+$ cells in tumor tissues, 3 fields/section, 3 sections/group. (**G**) The Kaplan–Meier estimator of metastasis-free survival in patients with BC, n=3,951.

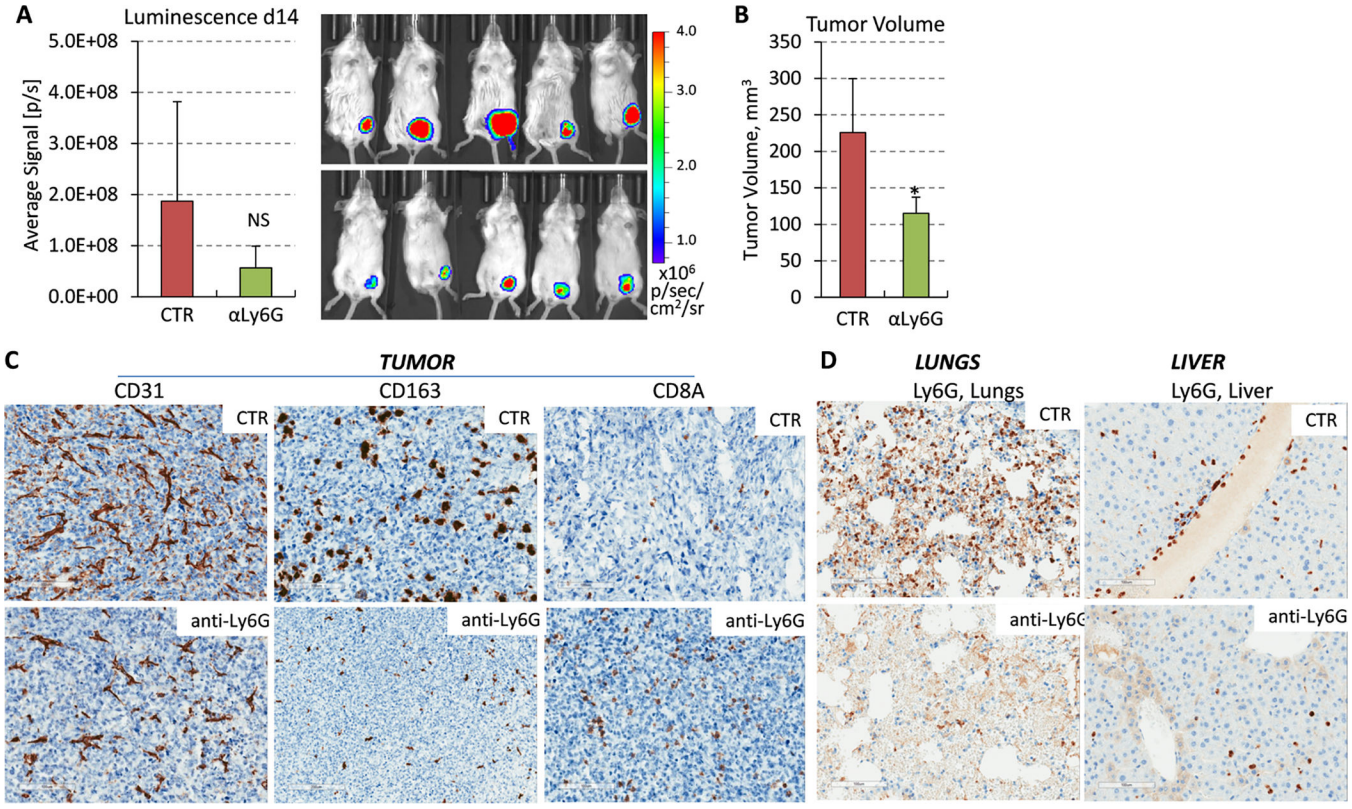

Figure 5. Depletion of PMN-MDSCs by anti-Ly6G antibody impedes the pre-metastatic niche.

(**A**) Panels show bioluminescence images and their quantification in live animals at day 14. 4T1-Luc mammary carcinoma cells (200,000) were orthotopically implanted in female BALB/c 6-week old mice, 7 mice/group. The next day, mice were administrated i.p. injections of vehicle-control (saline) or antibody to Ly6G scheduled on every other day. (**B**) Tumor volume at day 14. Statistical significance was determined using the two-tailed unpaired *t*-test (**P*<0.05). (**C**) Blood vessels (CD31), tumor-associated macrophages (CD163) and tumor-infiltrating T cells (CD8A) were visualized in tumor sections from comparable-size tumors (day 14) treated with anti-Ly6G or isotype-control (CTR) antibody, bar=100μm. (**D**) Panels show Ly6G stained sections of the lungs and liver of mice treated with anti-Ly6G or isotype-control (CTR) antibody, bar=100μm.

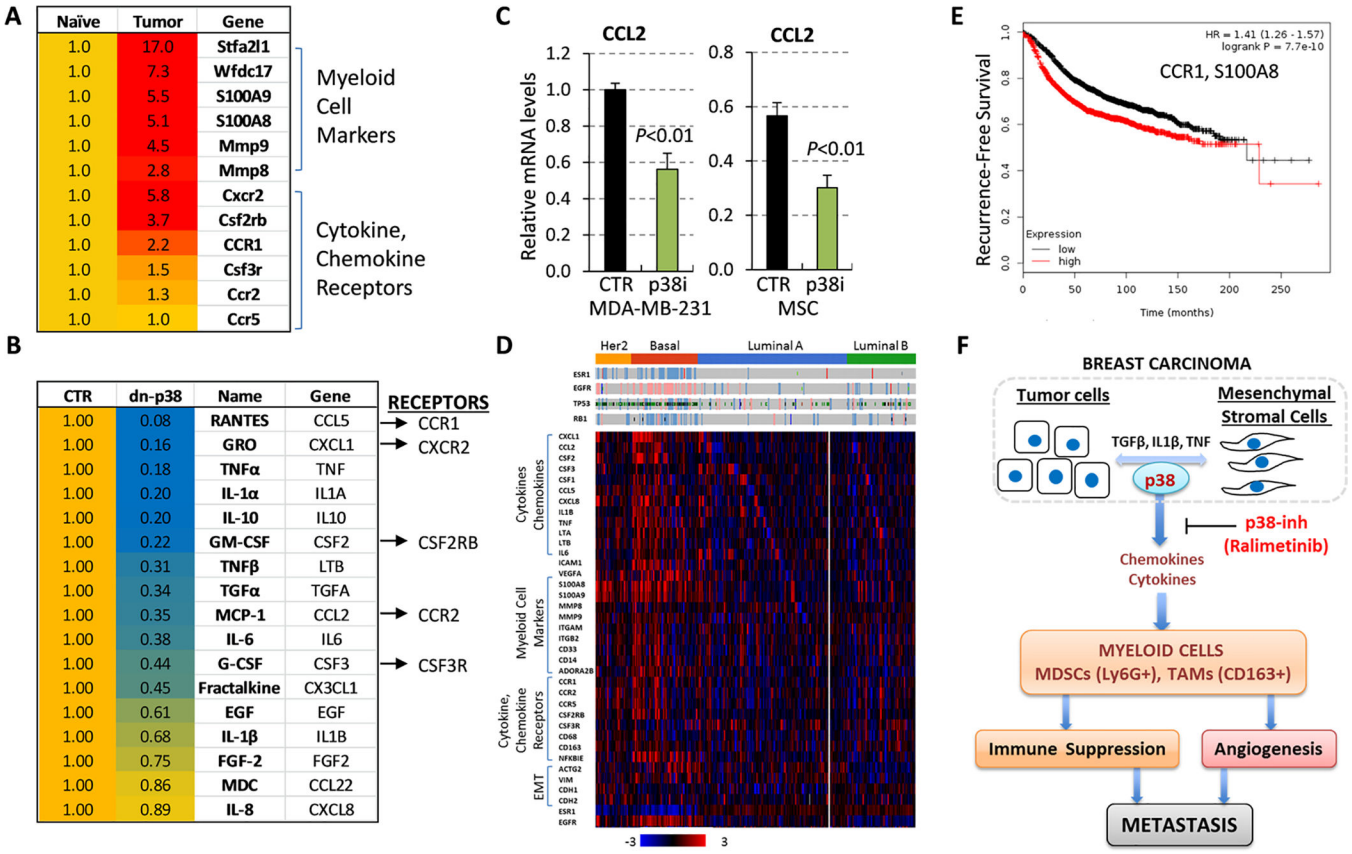

Figure 6. The p38 kinase controls the tumor-immune crosstalk that mediates the expansion of pro-tumor myeloid populations.

(**A**) Expression of myeloid cell markers and cytokine/chemokine receptors in the lungs from tumor-free (naïve) and 4T1 tumor-bearing mice (tumor). (**B**) Levels of secreted factors were measured in serum-free media conditioned for 48 hours by human MDA-MB-231 breast cancer cells, expressing the empty-vector (CTR) or dnp38 (dn-p38) constructs. Two biologically independent replicates were assayed using the Luminex 200 System. (**C**) Quantitative RT-PCR of CCL2/MCP-1 in total RNA from MDA-MB-231 and WI-38 mesenchymal stromal cells which were treated with vehicle (DMSO) or p38i (Ralimetinib) for 48 hours. (**D**) Expression profiles of breast cancer TCGA dataset. (**E**) Kaplan-Meier estimation of recurrence-free survival for CCR1 and S100A8 in BC patients (n=3,951). (**F**) The working model: the p38 kinase in tumor and mesenchymal stromal cells in the TME mediates expansion and mobilization of pro-tumor myeloid cells by controlling the tumor-immune crosstalk.